GEOLOGY | THE GEOLOGICAL SOCIETY OF AMERICA®

https://doi.org/10.1130/G52755.1

Manuscript received 11 September 2024
Revised manuscript received 30 October 2024
Manuscript accepted 21 November 2024

Published online 6 December 2024

Radiogenic heat production provides a thermal threshold for Archean cratonization process

Fawna J. Korhonen[1,*], David E. Kelsey[1], Tim J. Ivanic[1], Eleanore R. Blereau[1,2], R.H. Smithies[1,3], Matthew C. De Paoli[1], and Imogen O.H. Fielding[1]

[1]Geological Survey of Western Australia, 100 Plain Street, East Perth, WA 6004, Australia
[2]Department of Geology and Geological Engineering, Université Laval, Québec, G1V 0A6 Canada
[3]Timescales of Mineral Systems Group, School of Earth and Planetary Science, Curtin University, Bentley, WA 6102, Australia

ABSTRACT

A striking feature of the Yilgarn craton at the current erosional level is an abundance of late K-rich granites with radiogenic heat production elevated far above global crustal averages. Extrapolated back in time, the total thickness and contribution to crustal heat production and heat flow from these granites were greater, implying that the deeper crustal sources must also have had elevated radiogenic heat production. Through back-calculated and time-integrated one-dimensional thermal modeling underpinned by geological and geochemical constraints for the model crustal columns, we find that elevated radiogenic heat production provided a significant internal driver for prolonged crustal melting and eventual cratonization of the Yilgarn craton. Our results show that elevated thermal gradients driven by high heat production thermally primed the mid- and deep crust at or above the threshold for large-volume partial melting over long periods of time, as evidenced in the magmatic rock record. This would have been amplified by any additional heat that may have been provided by the mantle melting processes that punctuated the geological history. Over time, advective movement of progressively more radiogenic heat production to the shallower crust would have resulted in two complementary outcomes: progressively refractory deep crust and long-term cooling. The widespread granite "bloom" at 2650–2600 Ma records the final time at which the crust was fertile enough to melt in large volumes and the thermal gradient was hot enough to intersect the solidus. The magnitude of radiogenic heat production in the Yilgarn craton has been underestimated in previous studies, resulting in an underappreciation of the importance of its contribution to internal drivers of magmatism and ultimately cratonization.

INTRODUCTION

The processes by which cratonization of Archean crust occurred remain enigmatic (e.g., Cawood et al., 2013; Vanderhaeghe et al., 2019; Hawkesworth and Jaupart, 2021). A potentially undervalued role is that of radiogenic crustal heat production, particularly in priming the mid- and deep crust for large-volume partial melting and the ultimate transfer to the shallower crust. In the Yilgarn craton (Australia), cratonization was a prolonged process, with nearly continuous magmatism between 2830 and 2600 Ma. Final cratonization was characterized by a widespread late "bloom" of high-K granitic magmatism that peaked between 2660 and 2640 Ma with very high radiogenic heat production (interquartile range of 6.6–11.8 $\mu W/m^3$). Such prolonged magmatism, and particularly the late granite bloom, has been inferred to have been mantle driven (e.g., Bodorkos and Sandiford, 2006; Mole et al., 2019), although it largely occurred over a time frame with negligible mantle input. However, previous studies likely underestimated the magnitude of radiogenic heat production in the Yilgarn craton and therefore ruled it out as being a major contributor to cratonization, instead favoring external drivers (e.g., Bodorkos and Sandiford, 2006). A comprehensive new geochemistry data set from the Yilgarn craton (Smithies et al., 2023, 2024) allows for a thorough assessment of the role of radiogenic heat production in facilitating magmatism and long-term stability, without the need for external (mantle) drivers. In this study, we aimed to address whether the radiogenic heat production caused a thermal regime in the mid- and deep crust near, at, or above the solidus, setting up a "threshold" scenario primed for protracted large-volume melting, followed by long-term cooling. To achieve this, we utilized large-scale data sets collected by the Geological Survey of Western Australia, including geochemistry and robust metamorphic constraints, integrated with a detailed stratigraphic and event framework (e.g., Mole et al., 2019; Ivanic et al., 2022) and crustal architecture, to perform one-dimensional (1-D) thermal modeling of the Archean evolution of the Yilgarn craton. More generally, protracted magmatism and late granite "blooms" recognized in other Archean cratons (e.g., Superior Province, Slave craton, Pilbara craton) may reflect the signature of the role of radiogenic heat production in cratonization.

Geological Background

The Yilgarn craton is dominated by Archean granite-greenstone terranes formed between ca. 3100 and 2600 Ma, including the Youanmi, Narryer, and South West terranes of the West Yilgarn craton, and the Eastern Goldfields superterrane made up of the Kalgoorlie, Kurnalpi, Burtville, and Yamarna terranes (Fig. 1). Although craton-wide magmatism, including the 2660–2640 Ma late granite bloom, affected all the terranes from ca. 2720 to 2600 Ma, the Eastern Goldfields superterrane is younger and more juvenile than the West Yilgarn craton (e.g., Champion and Cassidy, 2007; Wyche et al., 2012; Mole et al., 2019).

GEOCHEMISTRY DATA SET

An extensive, high-quality geochemical data set of 5545 unaltered felsic igneous rocks

*fawna.korhonen@demirs.wa.gov.au

CITATION: Korhonen, F.J., et al., 2025, Radiogenic heat production provides a thermal threshold for Archean cratonization process: Geology, v. 53, p. 222–226, https://doi.org/10.1130/G52755.1

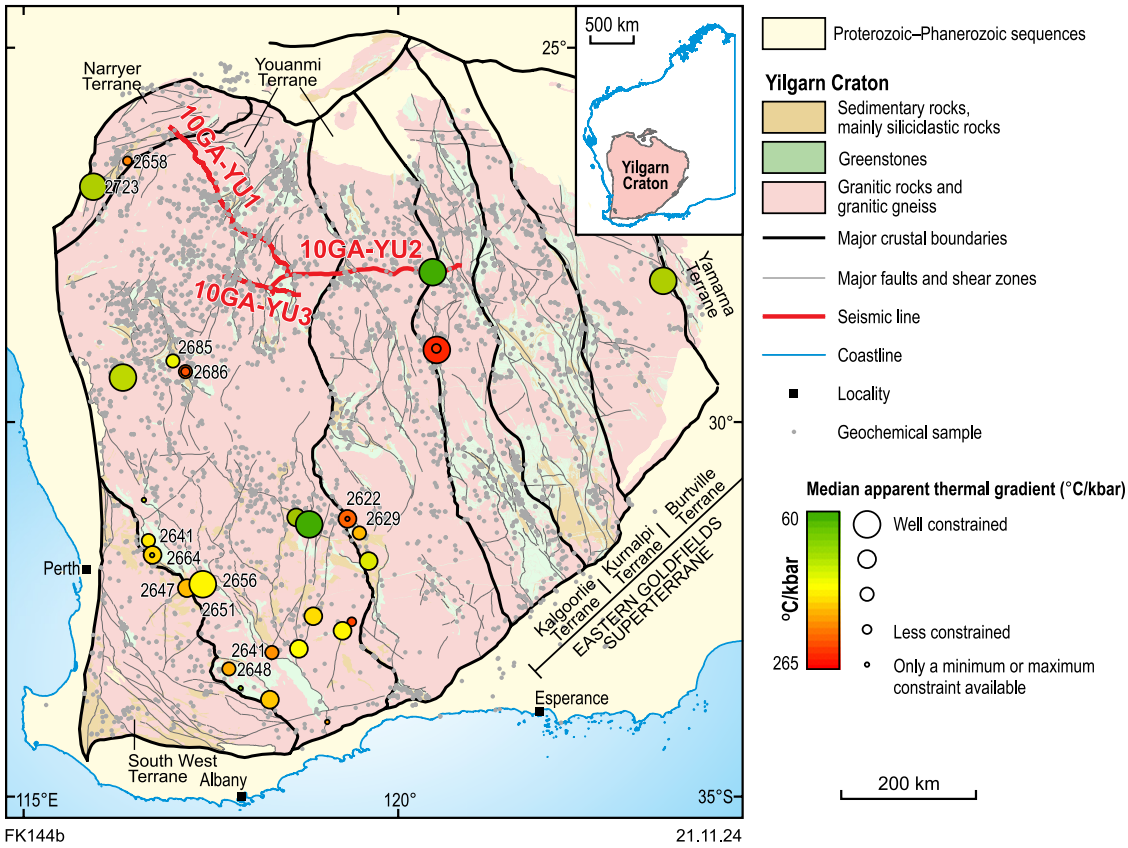

Figure 1. Simplified map of Yilgarn craton, showing geochemistry sample locations, Archean metamorphic data plotted as median peak apparent thermal gradient (with peak metamorphic age in Ma), and location of published seismic lines.

(Smithies et al., 2023, 2024; Table S1[1]) includes 522 dated (U-Pb zircon) samples, >90% of which have crystallization ages between ca. 2832 and 2600 Ma (Fig. S2). These can be divided (see Supplemental Material) into groups broadly reflecting:

1. Melting of mafic crust at deep-crustal (high-Ca, high-Sr/Y granites) and mid-crustal (high-Ca, low-Sr/Y granites) depths, equivalent to the sodic Archean tonalite-trondhjemite-granodiorite (TTG) series;

2. Melting, at a range of crustal depths, of variably reworked crustal sources (low-Ca granites), equivalent to typical Archean high-K granites but including a charnockitic variant (high-Ca [high-Ti] granites); and

3. Melting of a dominantly lithospheric mantle source (diorites, high field strength element granites, sanukitoids, syenites).

Additional geochemical data sets include lithologies that make up greenstone belts in the Youanmi terrane (Table S2; including banded iron formation, $n = 52$; felsic volcanic rocks, $n = 419$; mafic rocks, $n = 1835$; siliciclastic metasedimentary rocks, $n = 219$; ultramafic rocks, $n = 329$), and mafic igneous rocks (gabbro, $n = 30$; metagabbro, $n = 36$) from the Narryer terrane (Table S3), as a proxy for the mafic lower crust.

METAMORPHIC DATA SET

The West Yilgarn metamorphic data set comprises 30 samples (Fig. 1; Table S4). The methodology is outlined in the Supplemental Material. There are 14 samples with metamorphic ages ranging from ca. 2730 to 2622 Ma (Fig. 1) and 16 undated samples inferred to record Neoarchean metamorphism. The quantitative pressure-temperature (*P-T*) data reflect peak Neoarchean metamorphism at amphibolite- to granulite-facies conditions, consistent with previous work (e.g., Gee et al., 1981; Goscombe et al., 2019). The median peak metamorphic *T* ranges from 558 °C to 890 °C (Fig. S1A), and the median peak *P* ranges from 2.85 to 8.05 kbar (two outliers excluded; Fig. S1B). The median peak thermobarometric ratio ranges from 68 to 225 °C/kbar (Fig. 1). This data set provides *P-T* constraints through which model thermal gradients must pass.

HEAT PRODUCTION

Calculated heat production for the key lithological groups used in the 1-D models is provided in Figure 2, at present day (A_0) and at 2640 Ma (A_{2640}). The TTG group has median $A_0 = 1.80$ μW/m³, and high-K granite groups have median $A_0 = 5.15$ μW/m³, which is significantly higher than both the global average granite (= 2.5 μW/m³; Haenel et al., 1988) and the mean felsic value previously reported for the Yilgarn craton (= 1.88 μW/m³; Hawkesworth and Jaupart, 2021; Fig. 2A). The heat production map (Fig. 3A) shows that vast tracts of the exposed surface have A_0, which is significantly higher than global average granite. High heat production at the surface coupled with low to moderate surface heat flow (Fig. 3A) imply that modern-day heat production at depth must be lower, consistent with extraction of heat-producing elements (HPEs; K, Th, U) from deeper sources to produce these upper-crustal radiogenic granites. Median A_{2640} for the felsic groups ranges from 3.5 to 8.8 μW/m³ (Fig. 2B), and the heat production map for 2640 Ma (Fig. 3B) shows that the lithologies presently exposed would have had considerable heat production. Approximately 89% of the dated granites have calculated heat production at the age of crystallization (A_{Cryst}) > 2.5 μW/m³ (Fig. S2), with a gradual increase until the highest A_{Cryst} values in the high-K granite (= low-Ca granite groups) at 2680–2600 Ma.

THERMAL MODELING

To investigate the effects of radiogenic heat production on the Archean thermal evolution of the Yilgarn crust, 1-D numerical models were conducted. Model setups are shown in Figure 4A and explained in the Supplemental Material. For most lithologies, heat production was derived from age-corrected values calculated from the geochemical data set. However, for melt products derived from known sources,

[1]Supplemental Material. Details of geochemistry classification, analytical details for metamorphic data, details on heat production calculations, thermal modeling, Tables S1–S8, and Figures S1–S7. Please visit https://doi.org/10.1130/GEOL.S.27920472 to access the supplemental material; contact editing@geosociety.org with any questions.

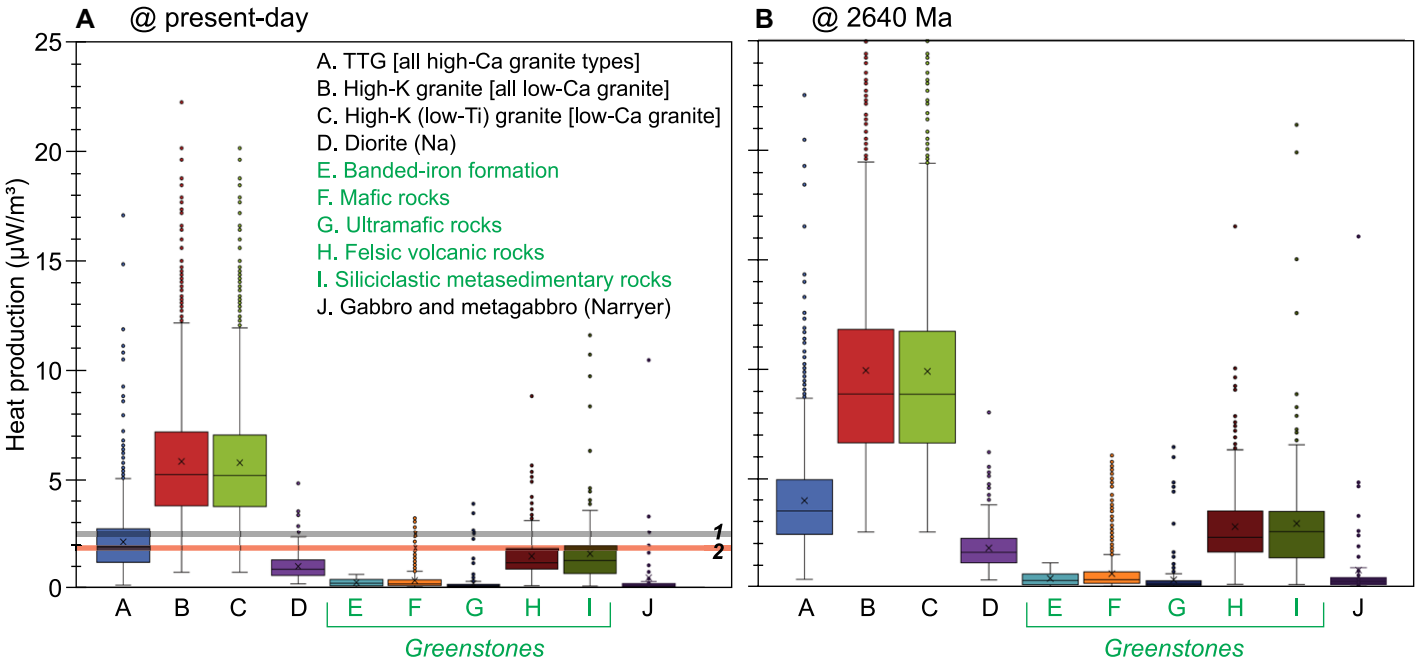

Figure 2. Box and whisker plots of heat production for select lithologies (with full classification provided in Fig. S4 [see text footnote 1]). (A) Present day. (B) 2640 Ma. Gray line (1) is average granite (= 2.5 μW/m³; Haenel et al., 1988); red line (2) mean felsic value for Yilgarn craton (= 1.88 μW/m³; Hawkesworth and Jaupart, 2021). Note some extreme outliers plot beyond range shown. TTG—tonalite-trondhjemite-granodiorite.

a proportion of the vertically integrated heat production was removed from each of the sources. Steady-state models were run at present day and at three different time intervals, broadly capturing key stages when the crustal column had significant changes to its configuration: 2900–2760 Ma (model 1), 2760–2650 Ma (model 2), and 2650–2600 Ma (model 3). The predicted thermal gradients are intended to represent the end of each model, although the absolute age at which the system reaches steady state could be different, especially for model 3. There are two results for model 3: one based only on heat production as a thermal source (solid red line, Fig. 4B), and one that also includes the advective thermal effects of high-K granite emplacement (dashed red line, Fig. 4B). Other thermal perturbations, such as mafic underplating or intru-

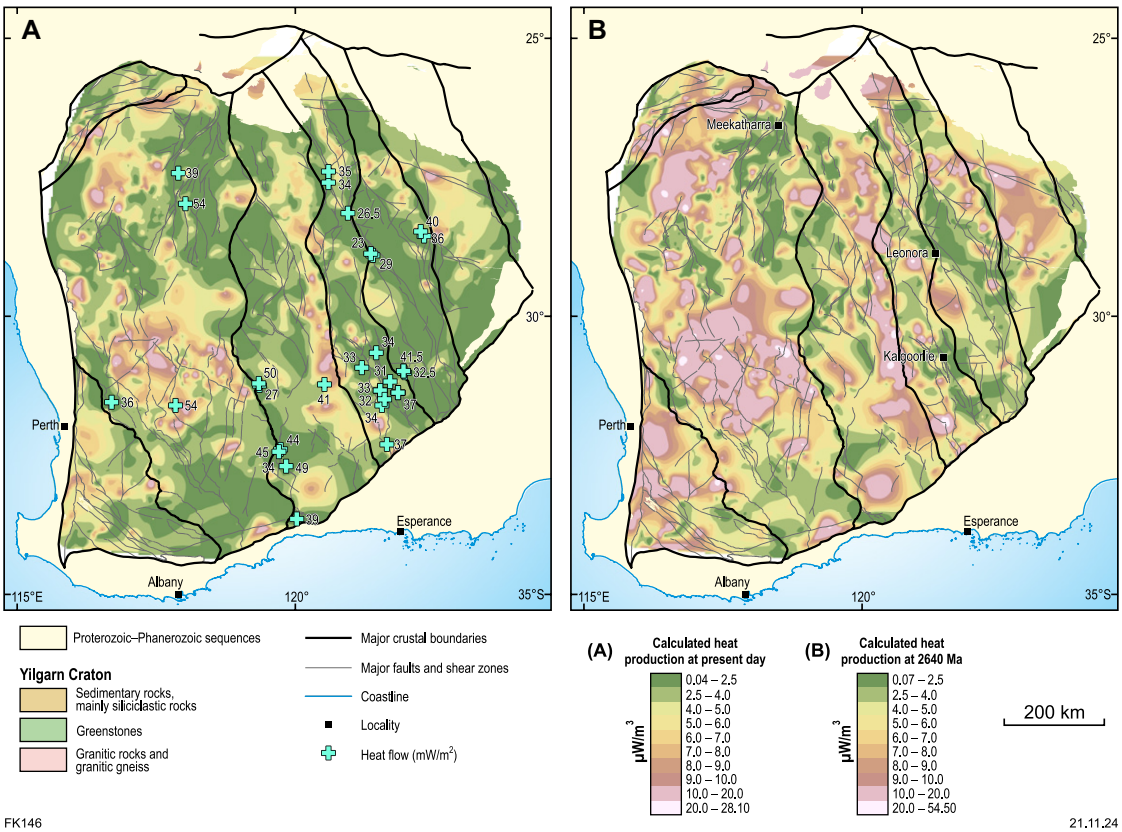

Figure 3. Heat production maps of Yilgarn craton, based on whole-rock geochemistry of least-altered samples. (A) Present day, with surface heat flow. (B) Heat production calculated at 2640 Ma. Maps were generated with natural neighbor interpolation using natural breaks in data values.

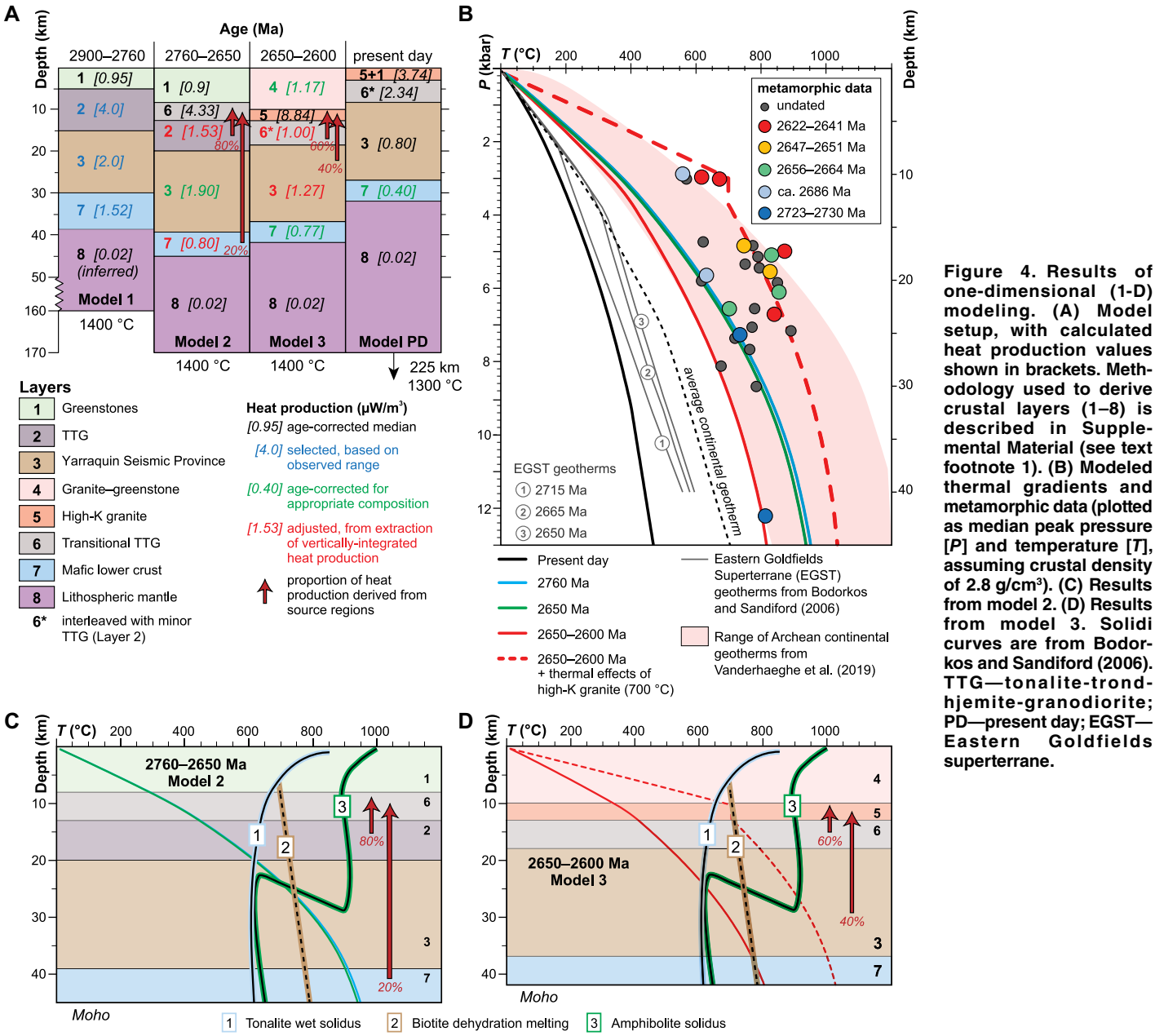

Figure 4. Results of one-dimensional (1-D) modeling. (A) Model setup, with calculated heat production values shown in brackets. Methodology used to derive crustal layers (1–8) is described in Supplemental Material (see text footnote 1). (B) Modeled thermal gradients and metamorphic data (plotted as median peak pressure [*P*] and temperature [*T*], assuming crustal density of 2.8 g/cm³). (C) Results from model 2. (D) Results from model 3. Solidi curves are from Bodorkos and Sandiford (2006). TTG—tonalite-trondhjemite-granodiorite; PD—present day; EGST—Eastern Goldfields superterrane.

sion, are not considered in any of the models, nor is the thermal dependence on conductivity considered; thus, the predicted thermal gradients can be treated as minimum values.

The models attempt to reconstruct a simple but realistic crustal evolution based on the existing stratigraphic and magmatic framework, with the sampled rocks providing constraints on crustal compositions. There are three important premises in the model setups: First, radiogenic heat production of many of the crustal components is well above global averages (Fig. 2). Second, the models are internally consistent, apart from the transitional TTG layer in the present-day setup that has an increase in A_0 relative to model 3 (Fig. 4A). Possible explanations are addressed in the Supplemental Material. Third, the high-K granitic rocks that characterize the late granite bloom have the highest radiogenic heat production and must have played a fundamental role in cratonization. Sandiford et al. (2001) and Sandiford and McLaren (2006) recognized that the thickness of high-heat-producing layers is a critical factor in the magnitude of their contribution to crustal heat flow and the consequent thermal regime, with thicker layers having greater influence. The 3-km present-day thickness of these radiogenic granites represents a minimum due to erosion, and therefore a minimum contribution to the total crustal heat production. Significantly, when extrapolating back in time, and to source regions for these granites, this thick layer implies that the Yilgarn crust contained elevated rates of heat production at depth prior to the late granite bloom. This agrees with recent work by Hartnady et al. (2024), which showed that fractionation of Th and U in the Yilgarn craton accompanied crust formation and differentiation as early as 3.3 Ga, suggesting that nearly the entire budget of these elements was part of the crustal profile by the Neoarchean, and that high-temperature metamorphism and crustal anatexis further redistributed HPEs.

IMPLICATIONS FOR CRATONIZATION

Numerous significant outcomes arise from the minimum thermal gradients in the 1-D models (Fig. 4). First, the ca. 2760 (model 1) and ca. 2650 Ma (model 2) thermal gradients are essentially the same (Fig. 4B), which depict elevated thermal conditions that intersect the tonalite wet solidus at ~20 km depth, and both dehydration curves at 25 km (Fig. 4C). This implies that for at least 100 m.y., the thermal regime of the mid- to deep crust was near to, at, or above conditions for partial melting. This protracted magmatism is evident in the geological record (e.g., Fig. S2), and it suggests that prolonged melting did not suf-

ficiently redistribute HPEs to reduce the thermal gradients until the next major crustal reconfiguration (model 3). This invites the possibility that the final granite bloom of high-K granites in model 3 (at ca. 2650–2600 Ma) occurred because the crust was thermally primed and subsequently crossed the tipping point. Second, after 2650 Ma (model 3), the crust was characterized by a cooling thermal gradient (Fig. 4B) due to the redistribution of significant radiogenic heat production at depths that were sufficiently shallow to lessen their thermal impact. The Nd isotope record for high-K granites in particular shows that older sources are more refractory than younger sources (Smithies et al., 2023), strongly suggesting that the deeper crust became progressively more refractory with time, as the thermal gradient progressively cooled. These factors would make it more difficult for the crust to melt, ultimately resulting in the cessation of melting and final cratonization by ca. 2600 Ma. Third, compared to the thermal gradients from Bodorkos and Sandiford (2006) for the Eastern Goldfields superterrane, there is a significant difference in thermal state (Fig. 4B). For example, in our models, the thermal gradient intersects the tonalite wet solidus at 20 km (at 2760–2650 Ma), whereas in Bodorkos and Sandiford (2006), it is 300 °C cooler at ca. 2715 Ma and 150 °C cooler at 2650 Ma, far below the solidus. Therefore, we consider that Bodorkos and Sandiford (2006) underestimated the contribution of radiogenic heat production to promoting large-volume melting and chemical differentiation of Yilgarn craton crust. Our revised finding highlights the value of the more comprehensive data sets available to us that have revealed the greater magnitude of an internal driver for cratonization, without the necessity for external thermal inputs.

The predicted thermal gradients at 2760–2650 Ma capture many of the metamorphic data points over that interval (Fig. 4B). However, the metamorphic record at 2641–2622 Ma appears, at first glance, to be at odds with the 1-D models. There is no realistic scenario for the magnitude and vertical distribution of radiogenic heat production that can explain this part of the metamorphic data set. However, as the metamorphic age data overlap with the ages of late "bloom" granites, and indeed many of the sampled metamorphic rocks are from among such granites, the metamorphic data may instead be explained by a thermal regime involving (significant) advective heat (dashed red line, Fig. 4B). That is, these granites caused an advective thermal regime superimposed on that caused by radiogenic heating alone and resulted in regional contact metamorphism, with Neoarchean thermobarometric ratios that lie at the extremes of the high-*T/P* regime of Brown and Johnson (2018).

CONCLUSIONS

Our results show that the thick layer of high-K, highly radiogenic granitic rocks currently exposed at the surface of the Yilgarn craton has significant implications for the thermal character and evolution of the craton. When integrated back in time to source rock types, radiogenic heat production was elevated in large parts of the Archean crustal column for protracted periods of time. This set up an internally driven thermal regime whereby the mid- and deep crust was at temperatures near or at the solidus from at least 2760 Ma, primed for (large-volume) melting, without the need to invoke external drivers for magmatism. This protracted melting and upward transfer of magma and heat-producing elements caused the crust to become more refractory over time, requiring progressively higher temperatures to continue melting and driving melting to shallower sources. This would have been a self-fulfilling process toward cratonization after 2650 Ma because upward migration of heat production combined with increasingly refractory deeper crust would have resulted in cooler and stronger crust (e.g., Sandiford and McLaren, 2006). Our models show that radiogenic heat internally primed the crust for cratonization—neither mantle heat nor other specific tectonic events were needed—and may account for the Archean trend from sodic to potassic granites preserved in the global record (e.g., Laurent et al., 2014).

ACKNOWLEDGMENTS

We are grateful to two anonymous reviewers and C. Kinney for constructive reviews on an earlier version of the manuscript and to T. Rushmer for editorial handling. The authors publish with the permission of the executive director, Geological Survey of Western Australia, and acknowledge funding from the Government of Western Australia Exploration Incentive Scheme.

REFERENCES CITED

Bodorkos, S., and Sandiford, M., 2006, Thermal and mechanical controls on the evolution of Archean crustal deformation: Examples from Western Australia, *in* Benn, K., Mareschal, J.-C., and Condie, K.C., eds., Archean Geodynamics and Environments: American Geophysical Union Geophysical Monograph 164, p. 131–147, https://doi.org/10.1029/164GM10.

Brown, M., and Johnson, T.E., 2018, Secular change in metamorphism and the onset of global plate tectonics: American Mineralogist, v. 103, p. 181–196, https://doi.org/10.2138/am-2018-6166.

Cawood, P.A., Hawkesworth, C.J., and Dhuime, B., 2013, The continental record and the generation of continental crust: Geological Society of America Bulletin, v. 125, p. 14–32, https://doi.org/10.1130/B30722.1.

Champion, D.C., and Cassidy, K.F., 2007, An overview of the Yilgarn craton and its crustal evolution, *in* Bierlein, F.P., and Knox-Robinson, C.M., eds., Proceedings of Geoconferences (WA) Inc. Kalgoorlie '07 Conference, 25–27 September 2007: Geoscience Australia Record 2007/14, p. 8–13.

Gee, R.D., Baxter, J.L., Wilde, S.A., and Williams, I.R., 1981, Crustal development in the Archaean Yilgarn block, Western Australia, *in* Glover, J.E., and Groves, D.I., eds., Archaean Geology: Second International Symposium, Perth, 1980: Geological Society of Australia Special Publication 7, p. 43–56.

Goscombe, B., Foster, D.A., Blewett, R., Czarnota, K., Wade, B., Groenewald, B., and Gray, D., 2019, Neoarchaean metamorphic evolution of the Yilgarn craton: A record of subduction, accretion, extension and lithospheric delamination: Precambrian Research, v. 335, https://doi.org/10.1016/j.precamres.2019.105441.

Haenel, R., Rybach, L., and Stegena, L., eds., 1988, Handbook of Terrestrial Heat Flow Density Determination: Dordrecht, Netherlands, Kluwer Academic Publishers, 486 p., https://doi.org/10.1007/978-94-009-2847-3.

Hartnady, M.I.H., Kirkand, C.L., Johnson, S.P., Smithies, R.H., Doucet, L.S., and Mole, D.R., 2024, Origin of Archean Pb isotope variability through open-system Paleoarchean crustal anatexis: Geology, v. 52, no. 1, p. 77–81, https://doi.org/10.1130/G51507.1.

Hawkesworth, C.J., and Jaupart, C., 2021, Heat flow constraints on the mafic character of Archean continental crust: Earth and Planetary Science Letters, v. 571, https://doi.org/10.1016/j.epsl.2021.117091.

Ivanic, T.J., Wingate, M.T.D., Lowrey, J.R., and Lu, Y., 2022, Formation of the Yilgarn Protocraton by Rift-Related Magmatism from 3.01 to 2.92 Ga: Geological Survey of Western Australia Report 232, 34 p.

Laurent, O., Martin, H., Moyen, J.-F., and Doucelance, R., 2014, The diversity and evolution of late-Archean granitoids: Evidence for the onset of "modern-style" plate tectonics between 3.0 and 2.5 Ga: Lithos, v. 205, p. 208–235, https://doi.org/10.1016/j.lithos.2014.06.012.

Mole, D.R., Kirkland, C.L., Fiorentini, M.L., Barnes, S.J., Cassidy, K.F., Isaac, C., Belousova, E.A., Hartnady, M., and Thébaud, N., 2019, Time-space evolution of an Archean craton: A Hf-isotope window into continent formation: Earth-Science Reviews, v. 196, 102831, https://doi.org/10.1016/j.earscirev.2019.04.003.

Sandiford, M., and McLaren, S., 2006, Thermo-mechanical controls on heat production distributions and the long-term evolution of the continents, *in* Brown, M., and Rushmer, T., eds., Evolution and Differentiation of the Continental Crust: Cambridge, UK, Cambridge University Press, p. 67–91.

Sandiford, M., Hand, M., and McLaren, S., 2001, Tectonic feedback, intraplate orogeny and the geochemical structure of the crust: A central Australian perspective, *in* Miller, J., Buick, I.S., Hand, M., and Holdsworth, R.E., eds., Polyphase Tectonism and Reactivation Mechanisms in Metamorphic Belts: Geological Society, London, Special Publication 184, p. 195–218, https://doi.org/10.1144/GSL.SP.2001.184.01.10.

Smithies, R.H., Lowrey, J.R., Champion, D.C., Lu, Y., and Gessner, K., 2023, Spatial Trends and Relationships Emerging from the Systematic Classification of Granitic Rocks of the Yilgarn Craton: Geological Survey of Western Australia Record 2023/5, 33 p.

Smithies, R.H., Gessner, K., Lu, Y., Kirkland, C.L., Ivanic, T., Lowrey, J.R., Champion, D.C., Sapkota, J., Masurel, Q., Thébaud, N., and Quentin de Gromard, R., 2024, Geochemical mapping of lithospheric architecture disproves Archean terrane accretion in the Yilgarn craton: Geology, v. 52, no. 2, p. 141–146, https://doi.org/10.1130/G51707.1.

Vanderhaeghe, O., Guergouz, C., Fabre, C., Duchêne, S., and Baratoux, D., 2019, Secular cooling and crystallization of partially molten Archaean continental crust over 1 Ga: Comptes Rendus Geoscience, v. 351, p. 562–573, https://doi.org/10.1016/j.crte.2019.07.002.

Wyche, S., Kirkland, C.L., Riganti, A., Pawley, M.J., Belousova, E., and Wingate, M.T.D., 2012, Isotopic constraints on stratigraphy in the central and eastern Yilgarn craton, Western Australia: Australian Journal of Earth Sciences, v. 59, no. 5, p. 657–670, https://doi.org/10.1080/08120099.2012.697677.

Printed in the USA